# Envelop-Climbing Locomotion Planning and Capability Analysis of a Deformable Tetrahedron Rolling Robot

Ziming Zhao, Yezhuo Li, Jianxu Wu, and Yan-an Yao

***Abstract*—This letter proposes an envelop-climbing locomotion planning for vertical obstacles by concave polyhedron construction in order to achieve high terrain adaptability of polyhedron robots. Using the triangle outline of the supporting area, a Z-shape path planning along the section of terrains is proposed. Three actions (Bridging, Enveloping and Climbing) for obstacle-crossing are sequentially planned and analyzed by constructing the external shape of concave polyhedrons to cover obstacles in the path. The kinematics analysis of the obstacle-crossing critical state for each action is established. The expression of central mass (CM), obstacle height and distance are deduced by homogeneous transformation matrix. The numerical solution of the maximum height along with motion angle and distance is figured out. Meanwhile, obstacles with different heights can be passed by executing a combination of the three different actions of the obstacle-crossing locomotion. The results of our analysis show that the locomotion can realize an obstacle-crossing ability with 170% of the height of CM. A prototype is manufactured to verify the envelop-climbing locomotion for obstacle-crossing (see video).**

***Index Terms*—Kinematics, mechanism design, obstacle-crossing capability, rolling robot, tetrahedron mechanism.**

## I. Introduction

POLYHEDRON mobile robot is a kind of polyhedral mechanism constructed by spatial linkages mechanism [1], [2], [3], [4]. By the deformation of the mechanism, it can realize mobility and adaptation on the ground [5], [6], [7], [8]. Based on the advantages of structure stability, simplest spatial shape and least actuators for omni-directional rolling, tetrahedron mechanism has been designed and studied extensively. NASA [9], [10] presented the TET-Walker robot with tetrahedral-based structure, which can deform and roll by changing the length of telescoping struts. Li et al. [11], [12], [13] proposed a tetrahedral mechanism with only revolute joints to gain larger work space and deformation. Usevitch et al. [14], [15] presented an untethered isoperimetric soft robot with the shape of an elongated square bipyramid, which was deformed and rolled by the roller modules moving on the inflated fabric tubes. Yim et al. [16], [17], [18] proposed a Variable Topology Truss, which can change the topology of the truss through self-reconfiguration.

The locomotion path planning for polyhedron robots has been researched. Aiming at the supporting area of polygon, path planning based on mesh generation is widely used [19], [20], [21], [22], which realizes a non-impact rolling locomotion algorithm, switching locomotion of robot and binary system control.

The obstacle-crossing ability is an important evaluation indicator for mobile performance of ground mobile robots. Traditional mobile robots rely on abnormal and transformable wheels to realize executing parts enveloping obstacles, which ensures the terrains passage capacity [23], [24], [25], [26], [27]. To general unstructured terrains, different from the passive adaptation of soft robots, the polyhedron robots can adapt the terrains actively by the switch of rigidity and flexibility on their path [28], [29], [30], [31], [32].

In our previous study, a deformable tetrahedron rolling mechanism (DTRM) with 6-URU branches was proposed [11]. Besides, a type of climbing actions with high central mass (CM) position for obstacle-crossing was proposed to cross obstacles by improving the CM position of mechanism with single degree-of-freedom (DOF) [33]. However, the climbing locomotion with high-CM increases the collision between the DTRM and the ground as it passes through obstacles. This makes the DTRM in the process of obstacle-crossing difficult to adjust or uncontrollable due to displacement errors and other problems. In addition, the single DOF motion can neither flexibly adjust the execution process of the action nor increase the deformation of DTRM, which limits its ability to overcome higher obstacles. By integrating the mechanism and the control system, the deformable tetrahedron rolling robot (DTRR) presented in this letter (Fig. 1) extends this work and can envelope its external shape as it advances for a more stable obstacle-crossing process and greater obstacle-crossing height. It measures 770.8 mm in length of links and weighs 10.2 kg.

This letter is organized as follows. The mechanical design of DTRR is presented in Section II. The kinematic and obstacle-crossing analysis of DTRR is presented in Section III, which

Manuscript received 5 April 2023; accepted 22 May 2023. Date of publication 8 June 2023; date of current version 23 June 2023. This letter was recommended for publication by Associate Editor E. Mingo Hoffman and Editor L. Pallottino upon evaluation of the reviewers' comments. This work was supported by the National Natural Science Foundation of China under Grant 52105006. *(Ziming Zhao and Yezhuo Li contributed equally to this work.) (Corresponding author: Yezhuo Li.)*

The authors are with the School of Mechanical, Electronic and Control Engineering, Beijing Jiaotong University, Beijing 100044, China (e-mail: 21116018@bjtu.edu.cn; li_yezhuo@bjtu.edu.cn; wujx@bjtu.edu.cn; yayao@bjtu.edu.cn).

This letter has supplementary downloadable material available at https://doi.org/10.1109/LRA.2023.3284374, provided by the authors.

Digital Object Identifier 10.1109/LRA.2023.3284374

Fig. 1. Deformable tetrahedron rolling robot (DTRR).

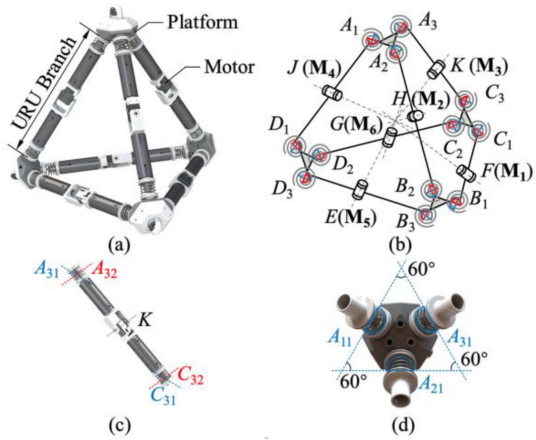


Fig. 2. Structure of DTRR: (a) 3D model; (b) sketch of the mechanism; (c) chain *AKC*; (d) positional relation between R joints connected to platform $A_{11}A_{21}A_{31}$.

determines the height of the passable obstacles and obstacle-crossing planning. The Experiments of rolling over different surfaces and climb over obstacles were presented in Section IV.

## II. Design and Manufacturing

The DTRR is illustrated in Fig. 2. The structure of the DTRR is composed of 4 platforms ($A_1A_2A_3$, $B_1B_2B_3$, $C_1C_2C_3$, $D_1D_2D_3$) and 6 URU chains ($A_1JD_1$, $A_2HB_2$, $A_3KC_3$, $B_1FC_1$, $B_3ED_3$, $C_2GD_2$).

Each chain has 2 binary links which are connected by revolute joint (R joint). The other side is connected to a platform by a universal joint (U joint). The motors are mounted at the R joints ($F$, $H$, $K$, $J$, $E$, $G$), which are named $\mathbf{M_1}$ to $\mathbf{M_6}$ in sequence, as shown in Fig. 2(b). The exterior shape of DTRR can be seen as a tetrahedron in the initial state. The DOFs of the tetrahedron robot is 12 [11].

### A. Robot Design

The sketch of DTRR is shown in Fig. 2(b). Chain $A_3KC_3$ and platform $A_1A_2A_3$ are taken as examples to show the relation of each kinematic joint. A U joint can be seen as 2 R joints in series orthogonal. Thus, to introduct the angle relation conveniently, all kinematic joints are replaced by R joints.

*1) The Chains:* One chain of DTRR contains 5 R joints and 2 links. As shown in Fig. 2(c), each R joint is named $A_{31}$, $A_{32}$, $K$, $C_{32}$ and $C_{31}$ from top to bottom. The axes of R joint $A_{32}$, $K$ and $C_{32}$ are parallel to each other, which are classified as one group. The axes of R joint $A_{31}$ and $C_{31}$ are parallel to one another, which are classified as another group. These 2 groups' axes are perpendicular.

*2) The Platforms:* After dividing the U joints into 2 R joints, the platforms can be supposed to connect with 3 R joints, as shown in Fig. 2(d). The axes of $A_{11}$, $A_{21}$ and $A_{31}$ constitute an equilateral triangle, which is in the same plane of the platform.

*3) The Main Mechanism:* The main body of DTRR acts like a tetrahedron when all middle revolute joints ($E$, $F$, $G$, $H$, $J$, $K$) are at an angle of 180 degrees, as shown in Fig. 2(a). The 4 platforms and 6 chains can be seen as the vertex corners and the straight edges of tetrahedron respectively. At the same time, the axis of each middle revolute joint intersects in a point, which is the body center of the tetrahedron.

### B. Actuation and Control

The DTRR is driven using six 14.8 Volts servomotors, which are mounted at R joints of the six chains. The servomotor is selected as Dynamixel MX-106R which is fitted with a 225:1 metal gearbox to produce a torque of 10.0 N·m. Although, 12 servomotors should be mounted to actuate the robot by DOFs analysis, our tests showed that using a semiflexible U joint which is composed of a spherical joint and a spring that is covered on it instead of each of the 12 U joints and actuate by 6 servomotors is sufficient. By the design of the semiflexible U joint, the revolution around axes $x$ and $y$ can realize the workspace from $-60$ degrees to 60 degrees, and around axis $z$ is limited to $\pm 30$ degrees. All the revolute directions have elastic restoring force, which made the movement of platforms can realize self-adjustment by terrains. The motors are powered using twelve 11.1 Volts, 3400 mAh lithium batteries. All the motors are controlled by a programmable Raspberry Pi 3B+. By using the programming feature of the transmitter, the actuated angle of each motor can be set by the kinematical result. The motors can reach $\pm 120$ degrees. Besides, the cameras can be installed in each platform to get the feedback of environment.

### C. Manufacturing

The DTRR mechanical structure is divided into 4 parts, named platform, semiflexible U joint, link and actuator. The platforms and all structural supporting members are 3D printed. The links of chains are using carbon fiber tubes which require high strength and light weight. The design is highly modular. The controllers are built-in platforms and the batteries in links, as shown in Fig. 3. Each part uses bolts and nuts to connect with each other, which are convenient for replacing the parts or changing the size of DTRR (a skilled operator needs about 2 minutes to replace one link of DTRR).

## III. Kinematic and Obstacle-Crossing Analysis

In this section, we analyze the kinematic and obstacle-crossing ability of the robot and present the device planning for climbing obstacles. The values of the actual robot used in the analyses were as shown in Table I.


Fig. 3. Main body of DTRR that has motors, the semiflexible U joints, the battery and electronics.

TABLE I
SPECIFICATIONS OF DTRR

| Definition | Variable | Value |
|---|---|---|
| Total length | — | 770.8 mm |
| Total width | — | 678.4 mm |
| Total height | — | 694.9 mm |
| Total mass | $m$ | 10.2 kg |
| Length of links | $l$ | 300 mm |

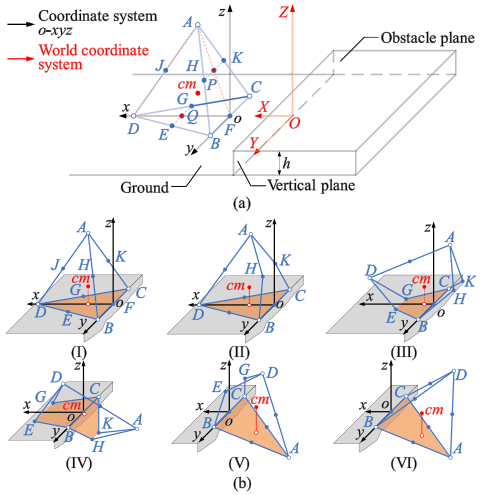


Fig. 4. Obstacle-crossing analysis model: (a) The definition of coordinate system and vertical obstacle; (b) the envelop-climbing locomotion.

### A. Kinematic Analysis

*1) Configuration and Terminology:* To describe and analyze conveniently, the sizes of platforms and links are ignored, which platforms $A_1A_2A_3$, $B_1B_2B_3$, $C_1C_2C_3$ and $D_1D_2D_3$ are simplified to point $A$, $B$, $C$ and $D$ respectively, as shown in Fig. 4(a). The passability of the robot is analyzed in this letter by taking the vertical obstacle as target obstacle, which includes the ground, the vertical plane and the obstacle plane, and $h$ is defined as the height of the vertical obstacle.

While the robot is in a tetrahedral state, let $F$ be the origin $o$ for rectangular system of the robot, which ***oD*** for $x$ axis, ***oB*** for $y$ axis and the line go through point $o$ and be straight up for $z$ axis. Then the Cartesian coordinate system $o$-$xyz$ for three-dimensional space has been established, which is defined as the coordinate system $o$-$xyz$, as shown in Fig. 4(a). The coordinate of each point can be represented as

$$p = \begin{bmatrix} p_A & p_B & p_C & p_D & p_H & p_K & p_E & p_G & p_F & p_J \end{bmatrix} \quad (1)$$

When the robot is on the ground and begins to cross the obstacle, let point $O$ be the intersection point of $x$ axis from coordinate system $o$-$xyz$ and vertical plane. The $x$ axis from coordinate system $o$-$xyz$ for $X$ axis, the intersection line of vertical plane and ground for $Y$ axis and the line go through point $O$ and be straight up for $Z$ axis. Then the Cartesian coordinate system $O$-$XYZ$ for three-dimensional space has been established, which is defined as a world coordinate system, as shown in Fig. 4(a). The coordinate of each point in $O$-$XYZ$ can be represented as $p'$.

*2) Envelop-Climbing Locomotion Planning:* According to the DOFs analysis and symmetric-drive rolling locomotion [11] of the robot, an envelop-climbing locomotion has been planned, which can envelop and adhere to the obstacle to realize self-adaptation. The locomotion can be described by $\mathbf{M_1}$ and $\mathbf{M_4}$ locking, $\mathbf{M_2}$ and $\mathbf{M_3}$ synchronously driving, $\mathbf{M_5}$ and $\mathbf{M_6}$ synchronously driving as examples, as shown in Fig. 4(b-I).

During the climbing locomotion, the chain $BFC$ is supposed to be fixed to the ground, which can be revolved around for the robot. Therefore, at the moments of Fig. 4(b-IV)–(b-VI), the robot is supposed to be stable, and would not keep revolving around the chains $BFC$ by gravity. The plane $BCGE$ and plane $BHKC$ form a concave polygon to envelop the obstacle, as shown in Fig. 4(b-IV). When link $BH$ and $CK$ attach the obstacle, motion $\mathbf{M_5}$ and $\mathbf{M_6}$ contrarotate immediately to keep enveloping the obstacle and deform the mechanism to keep CM moving forward, which can adhere to the ground and decrease the contact from the ground.

Let $\theta_1 \sim \theta_6$ denote the drive angle of $\mathbf{M_1} \sim \mathbf{M_6}$ respectively. $\mathbf{M_2}$ and $\mathbf{M_3}$ at points $F$ and $J$ are named the first actuator group, while the angles are named the first driving angle $\alpha$ ( $\angle$AHB=$\angle$AKC $= \alpha$). $\mathbf{M_5}$ and $\mathbf{M_6}$ at points $E$ and $G$ are named the second actuator group, while the angles are named the second driving angle $\beta(\alpha)$ ( $\angle$DEB=$\angle$DGC $= \beta(\alpha)$). The driving angle of $\mathbf{M_1}$ and $\mathbf{M_4}$ are set at 180 degrees and keep locking. A climbing cycle is completed from (I) to (VI) in Fig. 4(b).

*3) Kinematics:* In order to describe the climbing locomotion of DTRR, the kinematic has been analyzed. The moment in Fig. 4(b-IV) is used to show the whole kinematic analysis as an example. At this moment, the first actuator group keeps working which means $\alpha$ is decreasing. The second actuator group begins to work while $\beta(\alpha)$ starts to decrease. The motion $\mathbf{M_1}$ and $\mathbf{M_4}$ are still locking. Based on the coordinate system $o$-$xyz$, the kinematic is analyzed.

During the locomotion, based on the relation of each kinematic joint, the geometry relation can be used to figure out the coordinate of each point, as

$$\begin{cases} \|\boldsymbol{AH}\| = \|\boldsymbol{BH}\| = \|\boldsymbol{BE}\| = \|\boldsymbol{DE}\| = l \\ \|\boldsymbol{AB}\| = 2l\sin\frac{\alpha}{2} \\ \|\boldsymbol{BD}\| = 2l\sin\frac{\beta(\alpha)}{2} \\ \|\boldsymbol{AD}\| = 2l \\ \boldsymbol{n_{ABH}} \cdot \boldsymbol{CG} = 0 \\ \boldsymbol{n_{CDG}} \cdot \boldsymbol{AH} = 0 \end{cases} \quad (2)$$

where "$\|\ \|$" is 2-norm and it can be represented to the length of link. Each of the equations in (2) is linearly independent to each other. Then $p$ can be solved as $p(\alpha)$. The planning of climbing locomotion is based on statics analysis. Therefore, the CM can

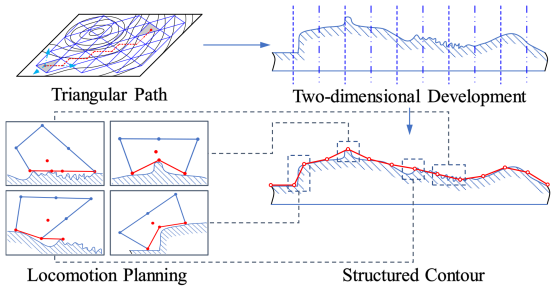


Fig. 5. Terrains dividing, structuralizing and locomotion planning.

be moved by robot deformation. According to the result of the kinematic analysis, the coordinate of *CM* is:

$$p_{cm} = \frac{1}{6}\left[p_{A_x} + p_{D_x} + p_{H_x} + p_{E_x} \quad 0 \quad p_{A_z} + p_{D_z} + p_{H_z}\right]^T \tag{3}$$

## B. Obstacle-Crossing Planning

Based on the triangular supporting area of the robot, the triangular grids with projection distortion nearby the obstacle is divided. The representing sets of triangular grids which contains the path are shown to be the geometric contour. The layered characteristic structured terrains are established by two-dimensional development. According to the contact of links and terrains, the structured contour is gained by dividing piecewise and linear fitting to each subsection, as shown in Fig. 5. Thus, the adaptive problem of moving over unstructured terrain is transformed into the passability problem of structured terrain.

Because of the symmetrical feature of climbing locomotion, the robot is symmetrical about plane *xoz*. To simplify the analysis, let each point project on plane *xoz*, the coordinate system *o-xyz* turns to *o-xz*, the world coordinate system *O-XYZ* turns to *O-XZ*. The 2 points' projections (*H*, *K*) are point *P*, the same as *E*, *G* to *Q* and *B*, *C* to *o*, as shown in Fig. 4(a).

The tetrahedron robot moves in a triangle gridding on the ground. The obstacle-crossing of vertical obstacles can be divided into three actions to cross different heights of obstacles, which are called bridging action, enveloping action and climbing action, as shown in Fig. 6(a). The bridging action is similar to a wheel mobile robot crossing vertical obstacle, in which the maximum height of obstacle depends on height of self-CM. The enveloping action is similar to human climbs wall sideward, which needs to envelope vertical obstacle itself by supporting the obstacle with hands. The CM of human is controlled to move forward and cross obstacles by the reaction force from the ground to the hands. The concave polygon configurational obstacle-crossing locomotion can be analyzed. The climbing action is similar to human walking on a single-step, which needs to bring a leg up and forward for moving. The two legs can be seen as links, which form to concave polygon to envelope the obstacle.

The robot executes rolling locomotion on the ground to adjust the distance with the obstacle, as shown in Fig. 6(b). After each action is finished, the position relationship of the robot with the obstacle will be judged. When facing cross obstacles, the robot

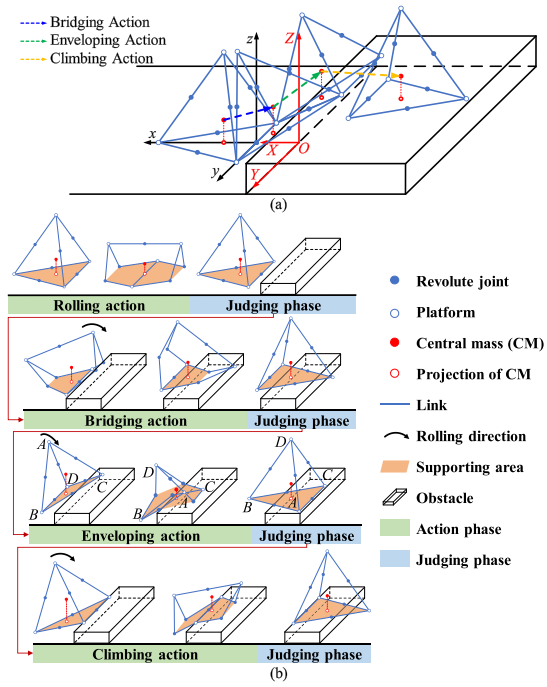


Fig. 6. Obstacle-crossing action planning: (a) Actions dividing; (b) locomotion planning.

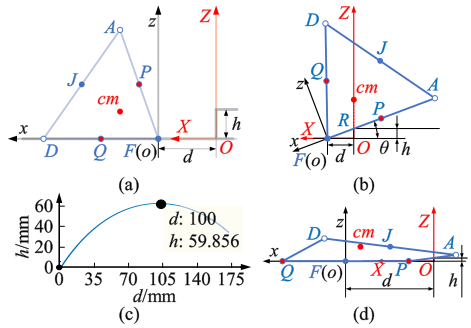


Fig. 7. Bridging Action: (a) The definition of *d* and *h*; (b) kinematics model when $d \leq l$; (c) relation between *d* and *h*; (d) kinematics model when $d > l$.

executes the bridging action on the ground. If it has succeeded to cross the obstacle, it turns to rolling locomotion on the ground. Otherwise it turns to the enveloping action to keep crossing obstacles. Then it will cross the obstacle or turns to the climbing action. If in climbing action it fails to cross, the robot will turn to the start of the bridging action and change the path to move. The locomotion planning introduced above is assumed that the angle of link *BFC* and the vertical plane is 0. When the angle has values, the DTRR can realize the adjustment of distance and angle by keep executing the enveloping-climbing locomotion, which can be solved by path planning (see part II in video).

## C. Obstacle-Crossing Locomotion Analysis

*1) Bridging Action:* Because the robot is symmetrical in bridging action, the projection coordinate system can be used to analyze the locomotion. As shown in Fig. 7(a), *d* is defined as the distance from point *o* to vertical plane. The robot deforms

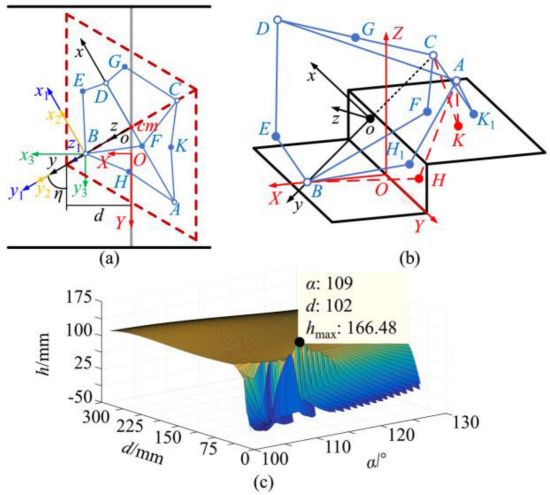


Fig. 8. Enveloping Action: (a) Kinematics model; (b) correct position; (c) relation between $d$, $h_{\max}$ and $\alpha$.

on the ground and the $z$ coordinate of point $P$ is not less than 0, then the climbing locomotion turns to symmetric-drive climbing locomotion. To describe the relationship of CM and obstacle conveniently, the homogeneous transformation matrix is used to transform the coordinate to world coordinate system.

When $d \le l$, as shown in Fig. 7(b), $\theta$ is equal to arctan($h$ / $d$). The link $FP$ intersects the obstacle at point $R$. The homogeneous transformation matrix is expressed as

$$\mathrm{T}_o^O = \begin{bmatrix} \mathrm{c}\theta & 0 & \mathrm{s}\theta & d \\ 0 & 1 & 0 & 0 \\ -\mathrm{s}\theta & 0 & \mathrm{c}\theta & 0 \\ 0 & 0 & 0 & 1 \end{bmatrix} \tag{4}$$

where s and c are the abbreviations of sin and cos functions correspondingly. The relation of $h$ and $d$ is

$$\begin{cases} p'_{cm_Z}(d) \ge h \\ p'_{cm_Z}(d) \le 0 \end{cases} \tag{5}$$

The relation curve of $h_{\max}$ and $d$ is shown as Fig. 7(c). When $d = 100$ mm, the $h_{\max}$ is 59.856 mm.

When $d > l$, as shown in Fig. 7(d). The $x$ coordinate of CM in the world coordinate system is less than 0 consistently, which means that can't realize obstacle-crossing. Then the robot turns to enveloping action.

*2) Enveloping Action:* The top view is used for analyzing to describe the position of each point in enveloping action conveniently. The world coordinate system $O$-$XYZ$ is redefined, in which the projection point $O$ from $B$ to vertical plane is the origin, $\boldsymbol{OB}$ for $X$ axis, the intersection line of vertical plane and ground for $Y$ axis and straight up for $Z$ axis, as shown in Fig. 8(a). Fig. 8(b) is shown for the moment which link $BC$ contact to the obstacle after robot falls from the critical phase, which $B$ on the ground and $C$ on the obstacle. At this moment, $d$ is defined as the distance $\|\boldsymbol{OB}\|$ from $B$ to the vertical plane. Some links will interfere with an obstacle when the critical phase of the robot in this moment, then points $H$ and $K$ are corrected with the help of semiflexible joints. Besides, to improve the stability of the

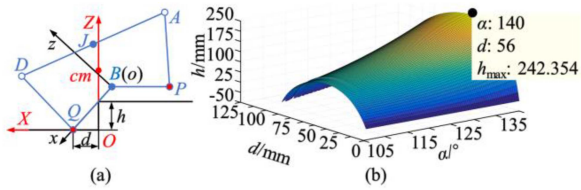


Fig. 9. Climbing action: (a) Kinematics model; (b) relation between $d$, $h_{\max}$ and $\alpha$.

robot in this moment, the motor in $F$ is actuating to let chain $BFC$ form to concave polygon to envelope obstacles, which the driving angle is named $\tau$. The corrected coordinate of CM is

$$p_{cm} = \frac{1}{12}\begin{bmatrix} 2p_{A_x} + 2p_{D_x} + 2p_{E_x} + p_{H_{1x}} + p_{K_{1x}} + p_{F_{1x}} \\ p_{H_{1y}} + p_{K_{1y}} \\ 2p_{A_z} + 2p_{D_z} + p_{H_{1z}} + p_{K_{1z}} + p_{F_{1z}} \end{bmatrix} \tag{6}$$

The homogeneous transformation matrix used to transform the coordinates to world coordinate system is shown as

$$\begin{aligned} \mathrm{T}_o^O &= T_{o_3}^O \mathrm{T}_{o_2}^{o_3} \mathrm{T}_{o_1}^{o_2} \mathrm{T}_o^{o_1} \\ &= \begin{bmatrix} \mathrm{c}\gamma & \mathrm{s}\gamma\mathrm{c}\eta & \mathrm{s}\gamma\mathrm{s}\eta & d - \|\boldsymbol{oB}\|\,\mathrm{s}\gamma\mathrm{c}\eta \\ -\mathrm{s}\gamma & \mathrm{c}\gamma\mathrm{c}\eta & \mathrm{c}\gamma\mathrm{s}\eta & -\|\boldsymbol{oB}\|\,\mathrm{c}\gamma\mathrm{c}\eta \\ 0 & -\mathrm{s}\eta & \mathrm{c}\eta & \|\boldsymbol{oB}\|\,\mathrm{s}\eta \\ 0 & 0 & 0 & 1 \end{bmatrix} \end{aligned} \tag{7}$$

where $\eta$ is defined by $\tan\eta = h$ / $d$ and $\gamma$ is equal to 60 degrees. Then the coordinates of CM are shown as

$$cm' = \mathrm{T}_o^O \cdot cm = \begin{bmatrix} x_{cm}\mathrm{c}\gamma + z_{cm}\mathrm{s}\gamma\mathrm{s}\eta - \|\boldsymbol{oB}\|\,\mathrm{s}\gamma\mathrm{c}\eta + d \\ -x_{cm}\mathrm{s}\gamma + z_{cm}\mathrm{c}\gamma\mathrm{s}\eta - \|\boldsymbol{oB}\|\,\mathrm{c}\gamma\mathrm{c}\eta \\ z_{cm}\mathrm{c}\eta + \|\boldsymbol{oB}\|\,\mathrm{s}\gamma \\ 1 \end{bmatrix} \tag{8}$$

When the CM of the robot moves over the vertical plane, the crossing condition is $x'_{cm} \le 0$ and $z'_{cm} > h$, which is

$$\begin{cases} x_{cm}\mathrm{c}\gamma + z_{cm}\mathrm{s}\gamma\mathrm{s}\eta - \|\boldsymbol{oB}\|\,\mathrm{s}\gamma\mathrm{c}\eta + d \le 0 \\ z_{cm}\mathrm{c}\eta + \|\boldsymbol{oB}\|\,\mathrm{s}\gamma > h \end{cases} \tag{9}$$

the robot can cross the obstacle. In (9), $\eta$ and $||\boldsymbol{oB}||$ are both the function of $\alpha$. The relation curve of $h_{\max}$, $d$ and $\alpha$ is shown as Fig. 8(c). When $\alpha = 109°$, $\beta = 111°$ and $d = 102$ mm, the $h_{\max}$ is 166.48 mm.

*3) Climbing Action:* There are two results after enveloping action. One is finishing the obstacle-crossing and keep rolling on the ground. The other one is failing to cross. By the judgment of falling back situation, the robot will turn back to bridging action or kee p doing climbing action. Fig. 9(a) shows the projection coordinate system of robot in the climbing action. In this moment, $d$ is defined as the distance from point $Q$ to the vertical plane, link $BQ$ intersects the vertical plane on point $N$, point $Q$ on the ground and point $N$ on the obstacle plane. The world coordinate system $O$-$XYZ$ is redefined, which the projection point $O$ from $Q$ to the vertical plane is the origin, $\boldsymbol{OQ}$ for $X$ axis, the intersection line of the vertical plane and ground for $Y$ axis and straight up for $Z$ axis, as shown in Fig. 9(a).

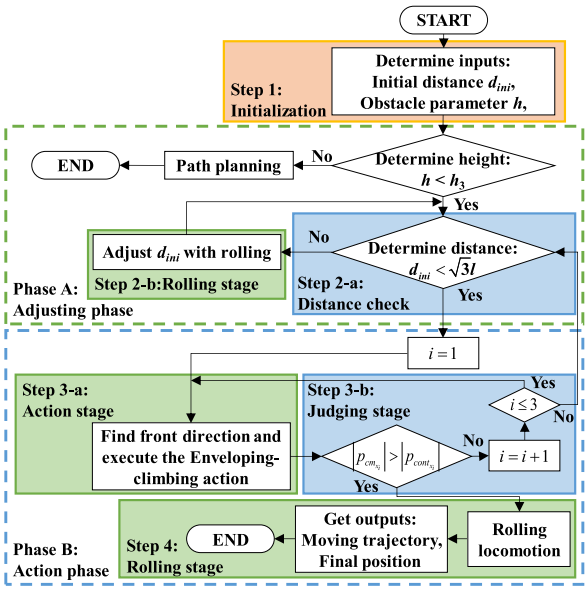


Fig. 10. Motion strategy of obstacle-crossing locomotion.

The homogeneous transformation matrix used to transform the coordinates to the world coordinate system is shown as

$$\mathrm{T}_o^O = \mathrm{T}_{o_2}^O \mathrm{T}_{o_1}^{o_2} \mathrm{T}_o^{o_1} = \begin{bmatrix} \mathrm{c}\theta & 0 & \mathrm{s}\theta & d - \|\boldsymbol{BQ}\| \mathrm{c}\theta \\ 0 & 1 & 0 & 0 \\ -\mathrm{s}\theta & 0 & \mathrm{c}\theta & \|\boldsymbol{BQ}\| \mathrm{s}\theta \\ 0 & 0 & 0 & 1 \end{bmatrix} \tag{10}$$

where $\theta$ is equal to arctan($h$ / $d$). Then the coordinates of CM are shown as

$$cm' = \mathrm{T}_o^O \cdot cm = \begin{bmatrix} x_{cm}\mathrm{c}\gamma + z_{cm}\mathrm{s}\gamma\mathrm{s}\eta - \|\boldsymbol{oB}\| \mathrm{s}\gamma\mathrm{c}\eta + d \\ -x_{cm}\mathrm{s}\gamma + z_{cm}\mathrm{c}\gamma\mathrm{s}\eta - \|\boldsymbol{oB}\| \mathrm{c}\gamma\mathrm{c}\eta \\ z_{cm}\mathrm{c}\eta + \|\boldsymbol{oB}\| \mathrm{s}\gamma \\ 1 \end{bmatrix} \tag{11}$$

When the CM of robot moves over vertical plane, the crossing condition is $x'_{cm} \le 0$ and $z'_{cm} > h$, which is

$$\begin{cases} x_{cm}\mathrm{c}\gamma + z_{cm}\mathrm{s}\gamma\mathrm{s}\eta - \|\boldsymbol{oB}\| \mathrm{s}\gamma\mathrm{c}\eta + d \le 0 \\ z_{cm}\mathrm{c}\eta + \|\boldsymbol{oB}\| \mathrm{s}\gamma > h \end{cases} \tag{12}$$

the robot can cross the obstacle. The relation curve of $h_{\max}$, $d$ and $\alpha$ is shown in Fig. 9(b). When $\alpha = 140°$, $\beta = 80°$ and $d =$ 56 mm, the $h_{\max}$ is 242.354 mm.

### D. Obstacle-Crossing Strategy

In order to enable DTRR to adjust its locomotion during crossing obstacles, instead of only moving according to preset driving parameters, a motion strategy for envelope-climbing locomotion is established as shown in Fig. 10. In Adjusting phase, the robot presets the action it needs to perform according to the height of the target obstacle. In Action phase, the robot detects the relationship between itself and the obstacle, and adjusts the action being performed based on this relationship. In this way, the parameters of experimental trajectories and theoretical trajectories can be compared many times in future research, so as to improve the motion process reasonably. Set the initial distance as $d_{ini}$, the obstacle parameter as $h$. Set $p_{cont}$ as the contact point between obstacles and links. And $h_i$ ($i =$ 12,3) means the maximum height in three actions respectively. Action I, II, III mean bridging, enveloping and climbing actions. The $x_i$ means the coordinate on axis $x$ in each action.

*Step 1.* Initialization: Set the initial distance as $d_{ini}$, the obstacle parameter as $h$. It is assumed that the bottom joints are instantaneously fixed to the ground to form the supporting area.

*Phase A.* Adjusting phase: This phase is used to adjust the position of DTRR to meet the execution conditions of envelop-climbing locomotion. The $h$ is compared with $h_3$. If $h$ is larger than $h_3$, it will turn to path planning and choose another path to move. Otherwise, it will switch to Action phase.

*Step 2-a.* Distance check: the DTRR compares $d_{ini}$ with the step length of the robot which equals to$\sqrt{3}$l. If it is larger than $\sqrt{3}$l, it will switch to Step 2-b to reduce the distance to obstacles. Otherwise, the envelop-climbing locomotion will be input as the next movement.

*Step 2-b.* Rolling stage: In this phase, the DTRR adjusts its position by rolling until it satisfies the distance check condition.

*Phase B.* Action phase: This phase is used to carry out the envelop-climbing locomotion. The cycle index $i$ is set as 1 firstly. The three envelop-climbing actions are executed as a circular strategy.

*Step 3-a.* Action stage: In the action stage, the DTRR first find the front direction. The envelop-climbing action is executed to climb the obstacle.

*Step 3-b.* Judging stage: The judging stage compares the CM position with the obstacle. The condition is used for judging if the CM is in the supporting area. If the conditions are satisfied, the DTRR has finished crossing the obstacle and the obstacle-crossing phase is finished to Step 4. Otherwise, the next action will be executed. When $i > 3$, it returns to Step 2-a to restart the obstacle-crossing strategy.

*Step 4.* Rolling stage: In this stage, the DTRR will roll away from the area of obstacle to finish the obstacle-crossing strategy.


Fig. 11. DTRR climbed an obstacle by bridging action. The height of obstacle is 70 mm and the initial distance is 100 mm.

## IV. Results

### A. Obstacle-Crossing Experiments

The DTRR experimental prototype is tested when crossing different height of obstacles in bridging action, enveloping action and climbing action. In all the experiments, the robot is controlled by a human operator (see video).

The experiment in Fig. 11 verified that the robot can climb an obstacle with a height of 70 mm and an initial distance of 100 mm by bridging action (see Fig. 11 and video). In Fig. 11(b),

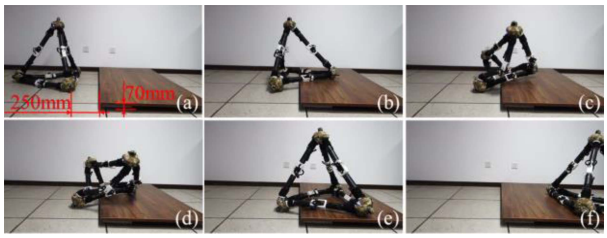


Fig. 12. DTRR climbed over an obstacle through a combination of bridging action and enveloping action. The height of the obstacle is 70 mm and the initial distance is 250 mm.

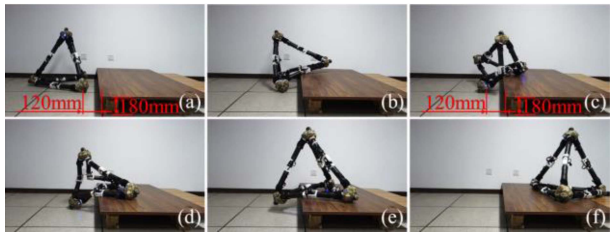


Fig. 13. DTRR climbed over an obstacle through a combination of bridging action and enveloping action. The height of the obstacle is 180 mm and the initial distance is 120 mm.

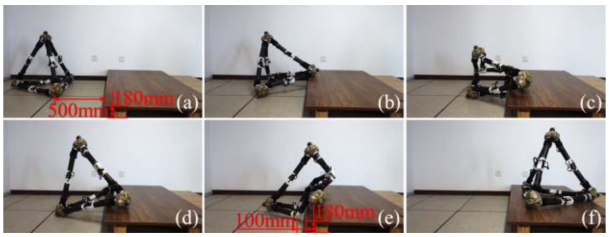


Fig. 14. DTRR climbed over an obstacle through a combination of the three actions. The height of the obstacle is 180 mm and the initial distance is 500 mm.

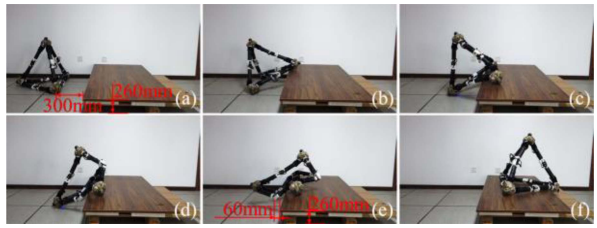


Fig. 15. DTRR climbed over an obstacle through a combination of the three actions. The height of the obstacle is 260 mm and the initial distance is 300 mm.

TABLE II
COMPARISON BETWEEN OBSTACLE-CROSSING EXPERIMENTS OF ENVELOP-CLIMBING LOCOMOTION

| Values | Theoretical | Experiment |
|---|---|---|
| CM height /(mm) | 144.887 | 155.14 |
| The max height of bridging action /(mm) ($\zeta$) | 59.856 (41.3%) | 70 (45.1%) |
| The max height of enveloping action /(mm) ($\zeta$) | 166.48 (114.9%) | 180 (116.0%) |
| The max height of climbing action /(mm) ($\zeta$) | 242.354 (167.3%) | 260 (167.6%) |


Fig. 16. DTRR rolling on unstructured environments.

the robot moved by symmetric-drive climbing locomotion until the 2 links contacted to the obstacle. In Fig. 11(c), the robot kept moving and the CM moved over the vertical plane. Then the robot deformed to a tetrahedron and the bridging action is finished.

The experiment shown in Fig. 12 verified the robot can cross an obstacle with a height of 70 mm and an initial distance of 250 mm. In Fig. 12(b), the CM of the robot could not get onto the vertical plane due to the excess of the required distance during the bridging action. Then the robot carried out enveloping action and crossed the obstacle when the $d$ is 120 mm as shown in Fig. 12(c)–(e).

As shown in Fig. 13, in this experiment the robot crossed an obstacle with a height of 180 mm and an initial distance of 120 mm in enveloping action. In Fig. 13(c), the robot deformed to the shape of a concave polyhedron to envelope the obstacle which increased the supporting area. In Fig. 14, the experiment verified the robot can cross an obstacle with a height of 180 mm and an initial distance of 500 mm. In Fig. 14(c), the robot did not satisfy the condition of distance and the CM could not reach the vertical plane in enveloping action. Then the robot moved in climbing action and crossed the obstacle with the $d$ of 100 mm by forming a concave polyhedron shape to envelope the obstacle, as shown in Fig. 14(e).

The experiment shown in Fig. 15 verified the robot can cross an obstacle with a height of 260 mm and an initial distance of 300 mm. In Fig. 15(e), the robot enveloped the obstacle by the deformation of the concave polyhedron which increased the supporting area. The $d$ is 60 mm which satisfied the condition of climbing the maximum height obstacle in theoretic analysis.

The maximum height of obstacle-crossing to the height of CM in tetrahedron ratio is defined as $\zeta$. The comparison between each obstacle-crossing experiment of envelop-climbing locomotion is shown in Table II. It can verify the theoretical analyses. The error between experiments and theoretical analyses is because of the shape of links and platforms. It can be solved by changing the shape or material of links and platforms. We use a correction coefficient summed up in experiments to solve this issue. It is used to multiply the theoretical value to acquire the maximum height of obstacle-crossing in the prototype and the theoretical value is used as a conservative estimate. According to the comparison between prototype experiments and theoretical analysis, the correction coefficient for the envelop-climbing locomotion is set as 1.08.

### B. Outdoors Experiments

Finally, we tested the robot outdoors on a variety of surfaces as shown in Fig. 16. The robot successfully crossed over grass, gravel, sand and rocky inclines. The robot also climbed over stones and concrete obstacles (see video). In Fig. 16(e), the robot crossed the common outdoor vertical obstacle with a height of 150 mm. The speed of the robot is 0.2 m/s and nearly unaffected by the surfaces it is crawling over.

## V. Conclusion

In this letter, an envelop-climbing locomotion planning for vertical obstacles by concave polyhedron construction in order to achieve high terrain adaptability of polyhedron robots is proposed. To realize the obstacle-crossing analysis, a kind of triangular grids with projection nearby the obstacle to unstructured terrains is divided. According to different heights of obstacles and distances of the robot, a kind of action combining obstacle-crossing analysis is presented. The 3 actions are called bridging, enveloping and climbing respectively. By deforming to a shape of concave polygon, the robot gains more supporting area to adapt to obstacles stably. A kinematic model is developed to analyze the maximum height of obstacle-crossing in each action. The robot can cross obstacles with 45.1%, 116.0% and 167.6% of CM height by executing a combination of different actions. Compared with the value of $\zeta$, which is the same definition and equals 144.8% in [33], the maximum $\zeta$ in envelop-climbing locomotion has been increased by 15.7%.

This study focuses on the maximum obstacle height and the corresponding obstacle-crossing strategy for DTRR. In the future, the influence of space constraints and the discrete rolling direction will be considered. The adaptation to the confined environment and the improvement of locomotion efficiency can be achieved through the design of local rotational DOFs (e.g., the combination of wheeled mechanism and tetrahedron mechanism can realize zero radius steering) and path planning. Moreover, the future goals also include the development of sensing system (touch sensor, depth camera, laser radar, et al.) and sensing strategy of the robot, and the improvement of path planning algorithm to realize autonomous sensing, decision making and movement. Then, the robot is able to autonomously cross unstructured terrains based on path planning.

## References


[1] K. Wohlhart, "Position analyses of normal quadrilateral Assur groups," *Mechanism Mach. Theory*, vol. 45, no. 9, pp. 1367–1384, 2010.

[2] K. Wohlhart, "Equally circumscribed cyclic polyhedra generalize platonic solids," *Mechanism Mach. Theory*, vol. 133, pp. 150–163, 2019.

[3] K. Wohlhart, "Double-ring polyhedral linkages," in *Proc. Interdiscipl. Appl. Kinematics Int. Conf.*, 2012, pp. 1–17.

[4] Y. B. Tian et al., "Multi-loop rover: A kind of modular rolling robot constructed by multi-loop linkages," *J. Mechanisms Robot.*, vol. 13, no. 1, 2020, Art. no. 011012.

[5] M. Yim, "New locomotion gaits," in *Proc. IEEE Int. Conf. Robot. Automat.*, 1994, pp. 2508–2514.

[6] M. Yim et al., "Modular reconfigurable robots in space applications," *Auton. Robots*, vol. 14, no. 2, pp. 225–237, 2003.

[7] J. Sastra, S. Chitta, and M. Yim, "Dynamic rolling for a modular loop robot," *Int. J. Robot. Res.*, vol. 28, no. 6, pp. 758–773, 2009.

[8] W. H. Lee and A. C. Sanderson, "Dynamic rolling of modular robots," in *Proc. IEEE Int. Conf. Robot. Automat.*, 2000, vol. 3, pp. 2840–2846.

[9] P. E. Clark et al., "BEES for ANTS: Space mission applications for the autonomous nanotechnology swarm," in *Proc. Amer. Inst. Aeronaut. Astronaut. 1st Intell. Syst. Tech. Conf.*, 2004, Paper. 6303.

[10] M. Abrahantes, A. Silver, and L. Wendt, "Gait design and modeling of a 12-tetrahedron walker robot," in *Proc. 39th Southeastern Symp. Syst. Theory*, 2007, pp. 21–25.

[11] Y. Z. Li et al., "A deformable tetrahedron rolling mechanism (DTRM) based on URU branch," *Mechanism Mach. Theory*, vol. 153, 2020, Art. no. 104000.

[12] Z. R. Wang et al., "Design and locomotion analysis of the tetrahedral mobile robot with only revolute joints (TMRR)," *Ind. Robot*, vol. 48, no. 4, pp. 614–625, 2021.

[13] R. Liu, Y. A. Yao, and Y. Z. Li, "Design and analysis of a deployable tetrahedron-based mobile robot constructed by Sarrus linkages," *Mechanism Mach. Theory*, vol. 152, 2020, Art. no. 103964.

[14] N. S. Usevitch et al., "An untethered isoperimetric soft robot," *Sci. Robot.*, vol. 5, no. 40, pp. 1–14, 2020.

[15] N. S. Usevitch, Z. M. Hammond, and M. Schwager, "Locomotion of linear actuator robots through kinematic planning and nonlinear optimization," *IEEE Trans. Robot.*, vol. 36, no. 5, pp. 1404–1421, Oct. 2020.

[16] E. Park, J. Bae, S. Park, J. Kim, M. Yim, and T. Seo, "Reconfiguration solution of a variable topology truss: Design and experiment," *IEEE Robot. Automat. Lett.*, vol. 5, no. 2, pp. 1939–1945, Apr. 2020.

[17] A. Spinos and M. Yim, "A linking invariant for truss robot motion planning," *IEEE Robot. Automat. Lett.*, vol. 7, no. 2, pp. 1424–1430, Apr. 2022.

[18] A. Spinos et al., "Topological reconfiguration planning for a variable topology truss," *J. Mechanisms Robot.-Trans. Amer. Soc. Mech. Engineers*, vol. 13, no. 4, Aug. 2021, Art. no. 040902.

[19] S. Park, E. Park, M. Yim, J. Kim, and T. W. Seo, "Optimization-based nonimpact rolling locomotion of a variable geometry truss," *IEEE Robot. Automat. Lett.*, vol. 4, no. 2, pp. 747–752, Apr. 2019.

[20] Y. Z. Li et al., "An agile assistant robot integrating operation and rolling locomotion," *Ind. Robot*, vol. 44, no. 1, pp. 114–126, 2017.

[21] Z. T. Wang, Y. Z. Li, and Y. A. Yao, "Motion and path planning of a novel multi-mode mobile parallel robot based on chessboard-shaped grid division," *Ind. Robot*, vol. 45, no. 3, pp. 390–400, 2018.

[22] R. Liu, Y. A. Yao, W. Ding, and X. P. Liu, "Locomotion optimization and manipulation planning of a tetrahedron-based mobile mechanism with binary control," *Chin. J. Mech. Eng.*, vol. 31, no. 1, pp. 1–22, Dec. 2018.

[23] Y. Kim, Y. Lee, S. Lee, J. Kim, H. S. Kim, and T. Seo, "STEP: A new mobile platform with 2-DoF transformable wheels for service robots," *IEEE/Amer. Soc. Mech. Engineers Trans. Mechatron.*, vol. 25, no. 4, pp. 1859–1868, Aug. 2020.

[24] T. Kislassi and D. Zarrouk, "A minimally actuated reconfigurable continuous track robot," *IEEE Robot. Automat. Lett.*, vol. 5, no. 2, pp. 652–659, Apr. 2020.

[25] Z. Tang, P. Qi, and J. S. Dai, "Mechanism design of a biomimetic quadruped robot," *Ind. Robot*, vol. 44, no. 4, pp. 512–520, 2017.

[26] T. F. Li, C. S. Zhang, S. J. Wang, and J. S. Dai, "Jumping with expandable trunk of a metamorphic quadruped robot–The Origaker II," *Appl. Sci.-Basel*, vol. 9, no. 9, May 2019, Art. no. 1778.

[27] J. X. Wu et al., "Design and analysis of a novel octopod platform with a reconfigurable trunk," *Mechanism Mach. Theory*, vol. 156, Feb. 2021, Art. no. 104134.

[28] L. Q. Yu et al., "Capability analysis and motion planning for obstacle negotiation of a closed five-bow-shaped-bar linkage," *J. Mech. Eng.*, vol. 53, no. 7, pp. 69–75, 2017.

[29] Y. Z. Li, Y. A. Yao, and Y. Y. He, "Design and analysis of a multi-mode mobile robot based on a parallel mechanism with branch variation," *Mechanism Mach. Theory*, vol. 130, pp. 276–300, 2018.

[30] Y. Y. He et al., "Design and mobility analysis of a multi-mode two-wheel mobile robot," *J. Mech. Eng.*, vol. 55, no. 23, pp. 83–92, 2019.

[31] F. Zhang et al., "A terrain-adaptive robot prototype designed for bumpy-surface exploration," *Mechanism Mach. Theory*, vol. 141, pp. 213–225, Nov. 2019.

[32] F. Zhang et al., "Physics-driven locomotion planning method for a planar closed-loop terrain-adaptive robot," *Mechanism Mach. Theory*, vol. 162, 2021, Art. no. 104353.

[33] Z. M. Zhao et al., "Obstacle-crossing gait planning of a tetrahedron mobile mechanism with 6-URU branch," *J. Mech. Eng.*, vol. 57, no. 23, pp. 85–96, 2021.